Received 26 October 2018; revised 25 December 2018; accepted 7 January 2019. Date of publication 15 January 2019; date of current version 1 March 2019. The review of this paper was arranged by Editor N. Collaert.

Digital Object Identifier 10.1109/JEDS.2019.2893299

Random Telegraph Noises in CMOS Image Sensors Caused by Variable Gate-Induced Sense Node Leakage Due to X-Ray Irradiation

CALVIN YI-PING CHAO [1] (Member, IEEE), THOMAS M.-H. WU [1], SHANG-FU YEH [1] (Member, IEEE), KUO-YU CHOU [1], HONYIH TU [1], CHIH-LIN LEE [1], CHIN YIN [1], PHILIPPE PAILLET [2] (Fellow, IEEE), AND VINCENT GOIFFON [3] (Member, IEEE)

1 Taiwan Semiconductor Manufacturing Company, Hsinchu 300-77, Taiwan
2 CEA, DAM, DIF, 91297 Arpajon, France
3 ISAE-SUPAERO, Université de Toulouse, 31055 Toulouse, France

CORRESPONDING AUTHOR: C. Y.-P. CHAO (e-mail: calvin_chao@tsmc.com)

ABSTRACT The effects of X-ray irradiation on the random noises, especially the random telegraph noises (RTN), of a 45-nm on 65-nm stacked CMOS image sensor with 8.3M 1.1 μm pixels are investigated. It is found that before X-ray irradiation the dominant type of RTN among the noisiest pixels is the source follower (SF) MOSFET channel RTN. In contrast, after X-ray irradiation up to a total ionizing dose of 1 Mrad(SiO_2), the RTN becomes dominated by the variable transfer-gate-induced sense node (SN) leakage. These two different types of RTN can be distinguished by their dependence on the transfer gate (TG) OFF voltage and the time between the correlated double sampling (CDS). The magnitude of the RTN from the variable SN leakage is proportional to the CDS time and can be suppressed effectively by increasing the TG OFF voltage, whereas the SF RTN is independent of the CDS time or the TG OFF voltage.

INDEX TERMS Random noise (RN), random telegraph noise (RTN), random telegraph signal (RTS), CMOS image sensor (CIS), pinned photodiode (PPD), active pixel sensor (APS), correlated double sampling (CDS), gate induced drain leakage (GIDL), variable junction leakage (VJL), variable retention time (VRT), radiation damage, X-ray, total ionizing dose (TID).

I. INTRODUCTION

The demand of higher resolution CMOS image sensors (CIS) with small footprint for high-end smartphone cameras continues to drive the pixel pitch down to the sub-micrometer regime (e.g., 0.9 µm [1]–[4], 0.8 µm [5]). For such small pixels, the light sensitivities and the full well capacities (FWC) are intrinsically limited by the pixel area. The FWC can be as small as 4,000 to 6,000 electrons. To achieve a high image quality, it is necessary to reduce the readout random noises (RN) to below a few electrons root-mean-square (e-rms) and the dark current (DC) to below a few electrons per second at 60 °C [1]–[4].

However, only achieving low average RN and DC may not be sufficient, since these defect-related parameters typically have long-tailed and highly non-Gaussian distributions. It is common that the RN and DC on the distribution tails could be 10 to 100 times higher than their average or median values. For continued manufacturing process improvement, it is important to understand the root causes of these long tails. A process enhancement improving the median RN does not necessarily lead to the reduction of the RN tail, vice versa, because the compositions and the physical origins of the noises in those two regions could be different.

Many studies have shown that the random telegraph noise (RTN) is the dominant noise on the RN distribution tail, which is the central subject of this study. A recent book on the random telegraph signals (RTS) in semiconductor devices may serve as a general reference to a wide range of topics [6].

2168-6734 © 2019 IEEE. Translations and content mining are permitted for academic research only.
Personal use is also permitted, but republication/redistribution requires IEEE permission.
See http://www.ieee.org/publications_standards/publications/rights/index.html for more information.

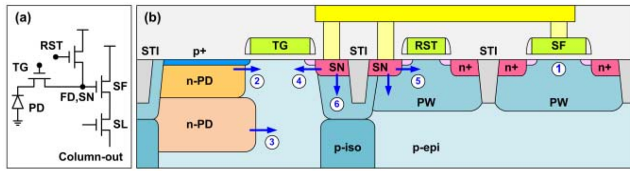

FIGURE 1. (a) The schematic of a 4T PPD active pixel. (b) The simplified cross section showing 6 potential RTN sources as described in Table 1. The arrows represent the leakage current directions.

The pinned photodiode (PPD) active pixels [8], [9] are almost universally used in today's CIS products. A 4-transistor (4T) pixel, as illustrated in Fig. 1(a), consists of a photodiode (PD), a transfer gate (TG), a reset gate (RST), a source follower (SF), and a row select device (SL). A variant of this structure is a 3-transister (3T) pixel without the SL, where the SF serves the dual functions of the signal buffering and the selection. The floating diffusion (FD) sense node (SN) is reset before the photo charge transfer; therefore, the reset KTC noises can be completely cancelled by the correlated double sampling (CDS) circuit technique. Another 3T non-PPD active pixel without the TG is also discussed for comparison purposes, where the reset noises cannot be fully cancelled due to the lack of CDS.

TABLE 1. Potential RTS/RTN sources in an active pixel.

Location	RTS/RTN source	4T†	3T†
SF	(1) SF MOSFET channel RTN	Y	Y
PD	(2) Variable transfer-gate-induced PD leakage (i.e., PD dark current)	Y‡	N‡
	(3) Variable non-gate-induced PD leakage (i.e., PD dark current)	Y	Y
SN	(4) Variable transfer-gate-induced SN leakage	Y‡	N‡
	(5) Variable reset-gate-induced SN leakage	Y	Y
	(6) Variable non-gate-induced SN leakage	Y	Y

† 4T: 4T PPD active pixel; 3T: 3T non-PPD active pixel without TG
‡ Y: yes, possible; N: no, not available

We may categorize the RTS/RTN into 6 varieties according to where it happens and how it happens, as illustrated in Fig. 1(b) and listed in Table 1. The 3 places where the RTS may be found in an active pixel are: the SF, the PD, and the SN. The first type of RTN is the MOSFET channel RTN, to be referred to as the MC-RTN [6] or the SF-RTN. The items 2 to 6 in Table 1 fall into the general category of the RTS/RTN due to variable junction leakage (VJL) [6]. In particular, items 2, 4, and 5 are the RTS/RTN related to the variable gate-induced drain leakage (GIDL) [10]–[20], which has been found responsible for the DRAM cell variable retention time (VRT).

The most common MC-RTN is generally caused by the random capture and emission of the conduction electrons in the SF channel by some traps near the interfaces between silicon and the gate oxide, or the shallow trench isolation (STI), or inside the bulk gate dielectric layer. The MC-RTN has been extensively studied either in the CIS or in the non-CIS test arrays or circuits [21]–[31].

The VJL is caused by the random switching of the leakage current among two or multiple discrete levels. The PD and the SN are the two nodes most sensitive to leakage, because they need to retain the photo charges during the integration time and the CDS time, respectively. In particular, the variable GIDL is likely due to the band-to-band or the trap-assisted tunneling in the high field region where the gate and the drain overlap [10]–[20]. The change of the occupancy status of a nearby trap may result in the discrete variation of the GIDL levels.

The RTS caused by the variable PD leakage is also called dark current RTS (DC-RTS) [32]–[43]. The DC-RTS could be caused by some meta-stable defects near the Si-STI interfaces, inside the Si bulk, or near the edge between the PD and the TG. In this work, we deliberately exclude the DC-RTS in order to simplify the observation and analysis. All the RN and SN leakage are measured with the TG turned off to disable the dark charge transfer.

The SN VJL is rarely observed or studied. The SN RTS due to the meta-stable Shockley-Read-Hall (SRH) type of generation-recombination (G-R) centers near the STI interface was briefly reported in [44]. The SN RTS due to the reset-gate GIDL was found responsible for the twinkling pixels in a 3T non-PPD CIS [45], [46]. The SN RTS due to radiation induced transfer-gate GIDL was recently reported mainly in the context of SN leakage and retention time [43] but its impact on the sensor output noise has not been reported or studied.

In this work we study the generation of RTN pixels due to X-ray radiation damage and the effects of total ionizing dose (TID) on these particular pixels. An RTN pixel is defined as a pixel with readout noise showing the RTS phenomenon. Our purpose is not to evaluate the radiation hardness of the chosen CIS against specific radiation sources. Rather, it is an extension of a general study of the RN and RTN in CIS where ionizing radiation is used as a tool to better understand the origins of the RTN pixels. This study could also lead to some insight into the potential process induced damage (PID) in CIS manufacturing.

Previously we reported that the dominant RTN in the studied CIS not exposed to any intentional radiation damage is the SF MC-RTN [29]–[31]. The key new finding of this study is that a different type of RTN is generated by the X-ray irradiation. Evidence shows that the RTN originates from the variable TG-gate-induced sense node leakage. For the samples exposed to high TID levels, the SN GIDL RTN dominates the pixel RN tail distribution. We did not observe any RST-gate-induced RTN in this work.

The rest of the paper is organized into the following sections. The CIS test chips and the noise performances are described in Section II. The TG negative bias and the effects on dark current are discussed in Section III. The observation of an increase of RN and RTN induced by X-ray irradiation and the link between RTN and GIDL is reported in

Section IV. The SN leakage levels before and after X-ray irradiation are reported in Section V. The direct verification that the RTN is due to variable SN leakage in time domain waveform is presented in Section VI. Finally, conclusions and closing remarks are given in Section VII.

II. TEST CHIP DESIGN AND PERFORMANCE

The chip under test is an 8.3 Mpixel (3,296×2,512), 1.1 μm pitch, stacked CIS. The top pixel-array wafer is fabricated in a 1P4M 45 nm backside illumination (BSI) process and the bottom ASIC wafer is fabricated in a 1P5M 65 nm low-power mixed-mode process. The simplified readout signal chain schematic is shown in Fig. 2(a). The pixel structure is a 2×2 4-shared version of the PPD active pixel without the select device (a total of 6 transistors in each 2×2 pixel group, i.e., 1.5T per pixel). There are no color filters or microlens.

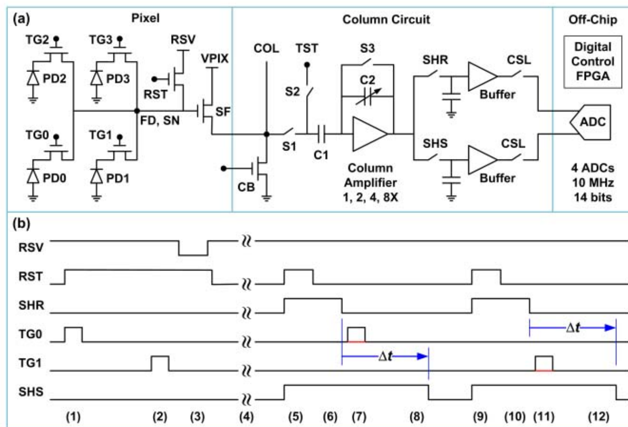

FIGURE 2. **(a) The simplified CIS signal chain circuits. (b) The operation timing diagram, where Δt is the programmable CDS time difference between the reset voltage sample/hold (SHR) and the signal voltage sample/hold (SHS).**

The pixel operation steps are described in Fig. 2(b) timing control diagram in the following sequence: (1) the even-column PD reset, (2) the odd-column PD reset, (3) deactivating the SF by pulling low the SN, (4) the rolling-shutter charge integration, (5) the SN reset, (6) the reset noise sampling, (7) the even pixel charge transfer, (8) the even pixel signal sampling, (9) the SN reset again, (10) the reset noise sampling, (11) the odd pixel charge transfer, and (12) the odd pixel photo signal sampling. The double-sampled reset and signal voltages are buffered and sent off chip to be digitized by external 14 bit analog-to-digital converters (ADC) at 10 MHz data rate. The operation voltages of this chip are tabulated in Table 2.

Although the reset KTC noises can be completely cancelled by CDS, the noises generated on the SN or the SF during the CDS time cannot be cancelled. Because, the double sampling of the reset voltage (SHR) and the signal voltage (SHS) are carried out at different times, one before

TABLE 2. **Operation voltages.**

RST ON voltage	3.1 V	RSV ON voltage	2.8 V
RST OFF voltage	0 V	RSV OFF voltage	0.7 V
TG ON voltage	2.8 V	VPIX (SF drain)	2.7 V
TG OFF voltage	–1.2 V	Analog circuit VCC	3.3 V

All other control signals are operated from rail to rail.

the charge transfer and one after. Thus, the associated noises are uncorrelated.

Three testing features are illustrated in Figs. 2(a) and 2(b). The first is that the charge transfer pulses (TG) may be disabled (red lines) during the CDS for dark RN measurements such that the readout noises are decoupled from the dark current shot noises and the DC-RTS. The second feature is that the time difference between the falling edges of the first and the second sampling, labelled as Δt, is programmable from 0 to 25 μs in 0.1 μs steps, which allows us to characterize the SN leakage and the CDS time dependence of the RTN.

Fig. 3 shows the input referred RN distribution for 7 chips before any X-ray irradiation. The RN is calculated as the RMS of 100 frames pixel by pixel. The median RN ranges from 1.29 to 1.32 e-rms under an 8X gain, which meets the requirement to achieve a 12-bit resolution for a FWC around 6,000 electrons. All 7 chips showed consistent performances with tight variations. This will be the benchmark to compare with the RN after X-ray irradiation.

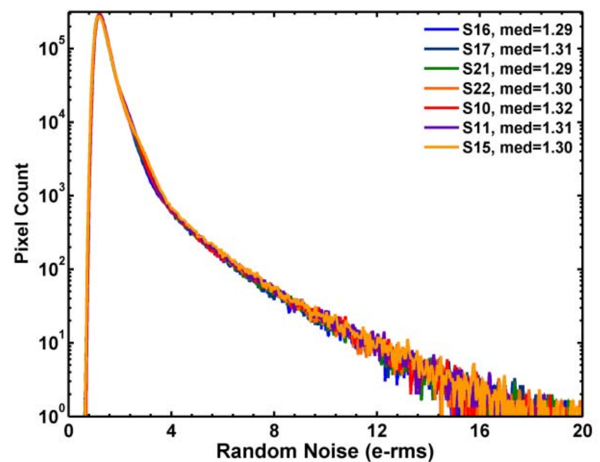

FIGURE 3. **The input-referred RN under an 8X analog gain for 7 chips without X-ray irradiation show consistent statistical behavior. The RN medians range from 1.29 to 1.32 e-rms.**

The third testing feature is that the readout circuit noises can be measured directly via a test-in input (TST) and bypass the pixel array by turning on switch S2 and turning off switch S1 in Fig. 2(b). The measured results are shown in Fig. 4, where the circuit noise distributions have nearly ideal Gaussian shapes (parabolas in the semi-log plot) without any long tails. The noise power is much smaller than the total RN including the pixels. With this, we may confidently conclude

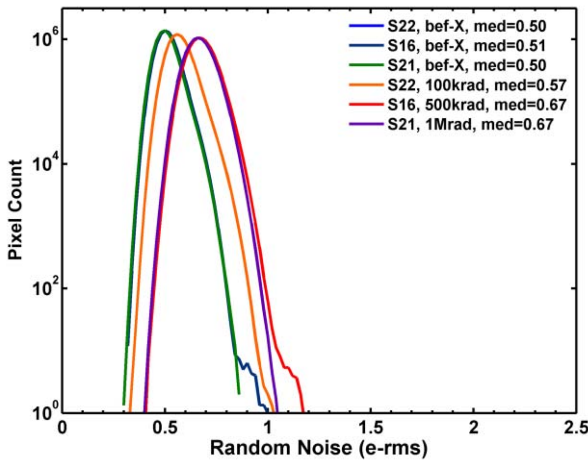

FIGURE 4. The circuit-only RN under an 8X gain, before and after X-ray irradiation. The RN medians range from 0.5 to 0.67 e-rms.

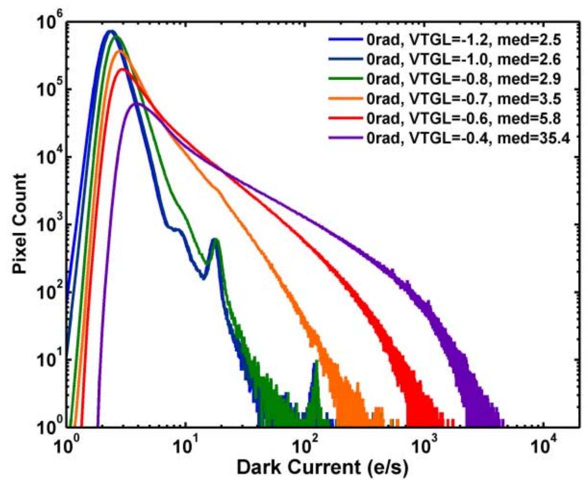

FIGURE 5. The dark current of an un-irradiated chip at 60 °C with the VTGL varying from −1.2V to −0.4V.

that the long tails of the whole chip RN distributions are indeed coming from the pixels, not from the circuits.

III. TRANSFER GATE OFF-VOLTAGE

The transfer gate OFF-voltage (VTGL) plays an essential role in this investigation. In fact, the VTGL is the key parameter allowing us to observe the GIDL effects on the SN leakage and the associated GIDL-RTN.

The TG is a custom-designed device to serve two important functions. When it is turned on it needs to ensure the complete charge transfer from PD to FD without any visible image lag. When it is turned off, it needs to have an extremely low OFF-current to prevent any carrier leakage into the PD.

For a standard 3.3V NMOS transistor of L = 0.38 μm in the 65 nm baseline technology, the OFF-current (at VGS = 0 V) is approximately 100 fA per micrometer of channel width. In contrast, for the 45 nm BSI process, the dark current of the 1.1 μm pixel at room temperature is smaller than 0.1 e/s, or 1.6×10^{-5} fA. Even taking into account the different bias conditions and device structures, the required TG OFF-current still needs to be several orders of magnitude lower than the standard NMOS OFF-current. For this reason, it is typically necessary to bias VTGL at a negative voltage such that the TG channel is in the accumulation condition and the leakage can be minimized by flooding the gate-silicon interface with high concentration of holes [47]–[54]. For this chip, the default VTGL is −1.2 V by design.

The dark current distributions before X-ray irradiation measured at 60 °C with the VTGL varying from −1.2 to −0.4 V are shown in Fig. 5. The median DC is around 2.5 e/s at the default VTGL = −1.2 V, and gradually increases as VTGL increases. The DC of the pixels on the distribution tail increases even faster than the median DC. This plot explains the importance of the negative VTGL bias. However, the price to pay is the high electrical field between TG and SN that may cause GIDL. These effects are to be discussed in the next 3 sections.

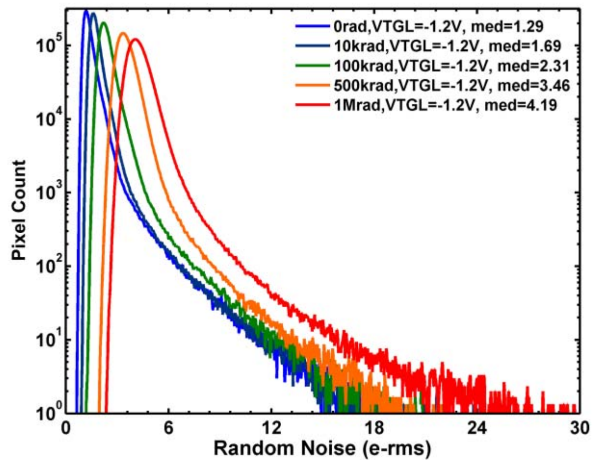

FIGURE 6. The RN distributions show systematic shift to higher values after the X-ray irradiation with 0, 10 krad, 100 krad, 500 krad, and 1 Mrad(SiO_2) TID.

IV. RANDOM NOISE AFTER X-RAY IRRADIATION

Ionizing radiation is known to lead to the generation of defects in the CMOS dielectrics and at their interfaces with silicon. Since RTN in CIS is attributed to oxide defects, X-ray irradiation is selected as a tool to investigate the mechanism and the origin of this noise. To do so, four packaged samples were exposed, while grounded, to 10 keV X-ray radiation at the CEA-DAM facility at room temperature. The total ionizing dose (TID) reached for each sample is 10 krad(SiO_2), 100 krad(SiO_2), 500 krad(SiO_2), and 1 Mrad(SiO_2), respectively.

The family of RN histograms before and after X-ray irradiation is shown in Fig. 6. Apparently there is a systematic increase of the RN as TID increases. The median noise increases from 1.29 e-rms before the irradiation to 4.19 e-rms after the 1 Mrad(SiO_2) irradiation. As proven in Fig. 4, the

radiation effects on the circuit noises are negligible, thus the increase of RN can be entirely attributed to the pixels.

The increase of RN in the major pixel population, near the mean and the median, is likely due to the increased flicker noises caused by the impact of radiation on interface defects. The increase of RN in the tail region is especially significant, and the distribution can no longer be approximated by the log-linear relationship as observed in the un-irradiated samples in Fig. 3. The inverse cumulative distribution functions (ICDF) plotted in Figs. 7 and 8 highlight the tails of the distribution with extremely low population densities that are difficult to show in histograms.

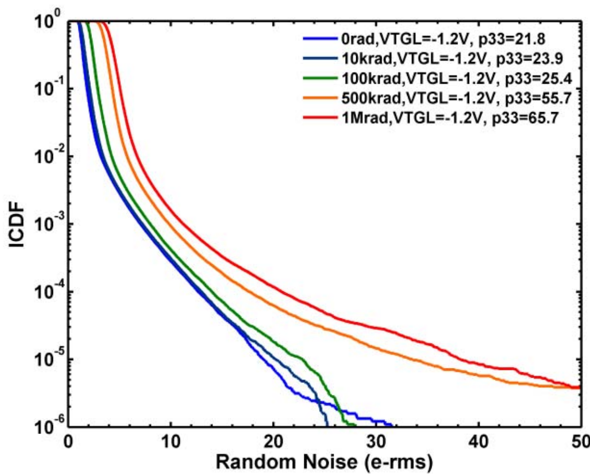

FIGURE 7. The inverse cumulative distribution functions (ICDF) of the RN under VTGL = −1.2 V. The p33 is the RN at ICDF = 3.3 ppm (3.3×10^{-6}).

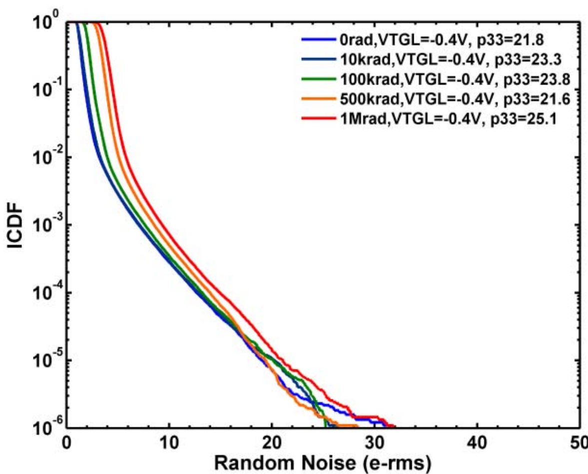

FIGURE 8. The inverse cumulative distribution functions (ICDF) of the RN under VTGL = −0.4 V. The p33 is the RN at ICDF = 3.3 ppm (3.3×10^{-6}).

Comparing the ICDF for VTGL = −1.2 V in Fig. 7 and the ICDF for VTGL = −0.4 V in Fig. 8, it is clear that the tail distribution of the RN is suppressed by the higher VTGL, as indicated by the RN at ICDF = 3.3 ppm in the legends. Under VTGL = −0.4 V, the RN tail returns to a shape roughly described by the log-linear relationship.

For comparison, we have verified that the RN distributions of the chips not exposed to X-ray irradiation are not affected by the VTGL voltages, as shown by the "0rad" curves in Fig. 7 and Fig. 8. This observation suggests that the nature of the RTN on the long tail generated by the X-ray radiation is different from that of the un-irradiated chip.

The increase of RN tail can be more clearly viewed in the plot of constant ICDF contours as a function of TID in Fig. 9. Especially in the TID range from 500 krad to 1 Mrad(SiO_2), a sharp increase of the RN is observed for ICDF = 1E–4, 1E–5, and 3.3E–6 contours.

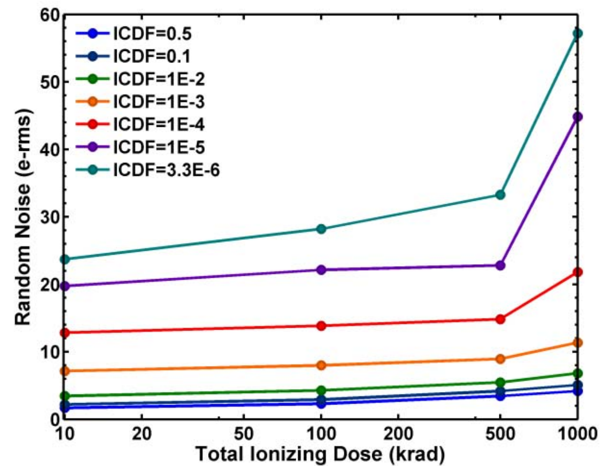

FIGURE 9. The RN constant ICDF contours as functions of the TID show accelerated increase from 500 krad to 1 Mrad(SiO_2).

The dependence of the RN of the noisier pixels on VTGL leads to the speculation that they are caused by the TG-induced SN leakage, related to the GIDL RTS, similar to that previously reported in DRAM cells [10]–[20]. When the VTGL is set to a more negative value, the electrical field between the SN and the TG is higher, which leads to higher GIDL and higher RTS amplitude that translates into high RN after the CDS operation. Such pixels with high noises coming from SN GIDL RTS are called GIDL RTN pixels in this paper.

We can practically separate the pixels with and without GIDL RTN by the correlation scatter plots of the RN under VTGL = −0.4V versus the RN under VTGL = −1.2V for the full 8.3 Mpixel array. The results are presented in Fig. 10 for TID levels of 0, 100 krad, 500 krad, and 1 Mrad(SiO_2), respectively. The cluster of data points along the "X = Y" diagonal line represent the pixels with RN nearly independent of VTGL. The cluster of data points on the right hand side branch of the "X = Y" line represents the pixels with higher RN under VTGL = −1.2 V than that under VTGL = −0.4 V.

The split of RN distribution into two branches evidently indicates that there are two kinds of RN or RTN sources, one dependent on VTGL and one independent of VTGL. The pixels with RTN dependent on VTGL will be considered as

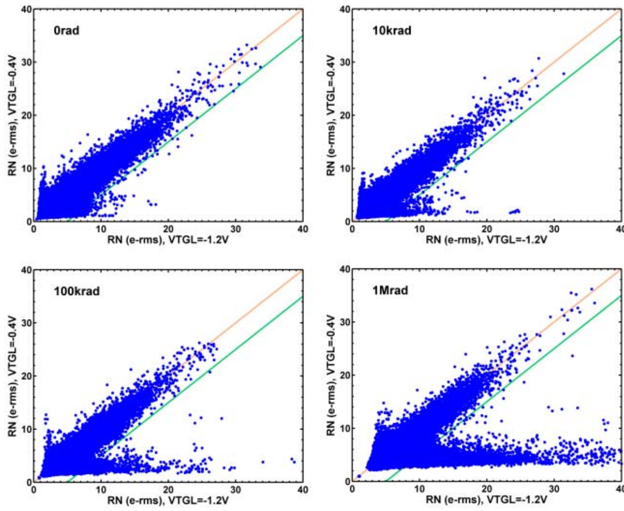

FIGURE 10. The correlation between the RN at VTGL = −0.4 V and the RN at VTGL = −1.2 V for the 8.3MP array after an increasing X-ray TID. The light red and the light green lines represent "X = Y" and "X = Y + 5 e-rms".

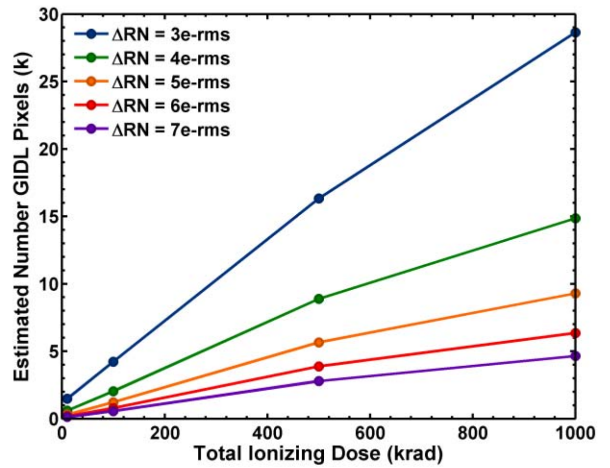

FIGURE 11. The number of GIDL pixels with the RN at VTGL = −1.2 V larger than the RN at VTGL = −0.4 V by a ΔRN ranging from 3 to 7 e-rms.

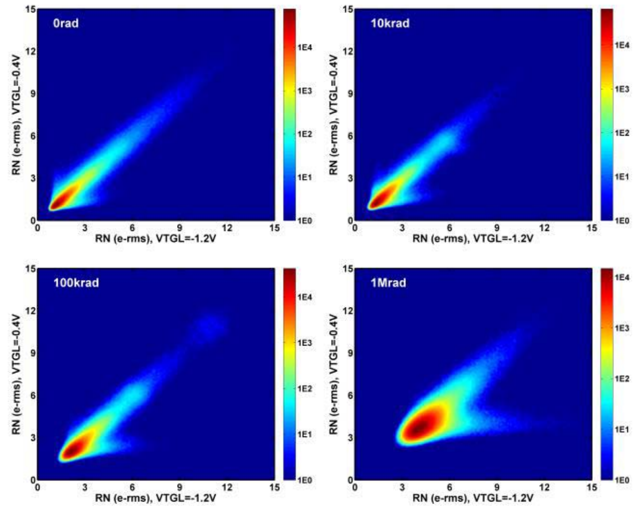

FIGURE 12. The 2D histograms of RN at VTGL = −0.4 V and the RN at VTGL = −1.2 V. The color bar shows the pixel count.

the GIDL RTN pixels. The pixels with the RTN independent of VTGL are mainly from the SF RTN. More direct evidence will be presented in Section VI.

We may estimate the number of GIDL RTN pixels by counting the number of data points on the right hand side of the "X = Y + ΔRN" line. Since there is no obvious cut-off between the RTN and non-RTN pixels, we use several empirical values for ΔRN, from 3 to 7 e-rms, for estimation. In Fig. 10 the "X = Y + 5 e-rms" light-green lines are drawn side by side with the diagonal light-red lines. The graph in Fig. 11 shows that the GIDL RTN pixel counts are approximately proportional to TID, which is intuitively consistent with the notion that the number of defects activated by the X-ray irradiation is proportional to the level of TID exposure. It is worthwhile to note that the estimated number of the GIDL RTN pixels is still a small portion of the total population, approximately less than 1 percent.

The scatter plots in Fig. 10 help us to differentiate the GIDL RTN pixels from the non-GIDL RTN pixels on the long tails where the population density is very low. For the densely populated region near the histogram peaks, such a separation does not clearly appear in the scatter plots. In Fig. 12, we zoom in these peak regions and use the 2-dimensional RN histograms to highlight the gradual splitting of the RN distributions as the TID level increases.

V. THE SENSE NODE LEAKAGE

In this section we focus on the SN leakage before and after X-ray irradiation and its dependence on VTGL. Since the RN is normally measured and specified at room temperature (RT), we also report the SN leakage at RT. On the other hand, the DC is conventionally quoted at 60 °C. Although we choose to exclude the DC-RTS in this study, it is still interesting to measure the DC as a function of TID for the purpose of comparing with the SN leakage. The measured DC after a TID from 0 to 1 Mrad(SiO_2) is shown in Fig. 13. Before X-ray irradiation the DC is about 2.7 e/s at 60 °C, a level comparable to those reported in [1]–[4]. The DC is increased to 256.5 e/s after a TID of 1 Mrad(SiO_2), almost 2 orders of magnitude higher than that without irradiation. The DC and DC-RTS may be a subject for future work. It is expected to be more complicated to analyze the data when the SF-RTN, GIDL-RTN, and DC-RTS are all present and mixed.

With respect to the DC, the SN leakage is seldom specified or quoted for any CIS product. The reason why SN leakage receives relatively less attention is probably because the charge retention time is typically longer for the PD (e.g., up to 1 second) while the charge retention time is only 25 μs in this design for the SN. Besides, as long as the CDS time is unchanged, the SN leakage only creates a fixed offset to the

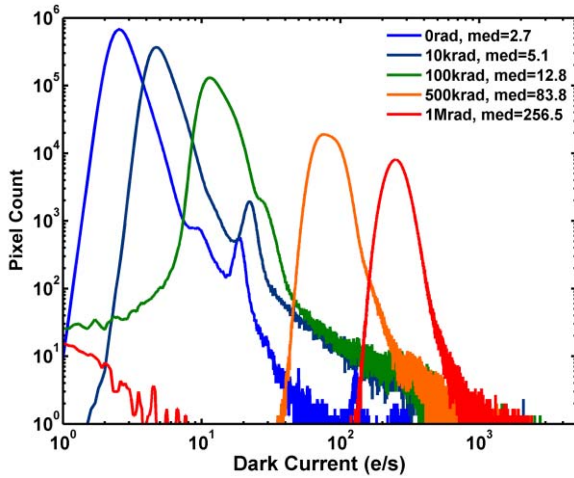

FIGURE 13. The dark currents at 60 °C for an X-ray TID level of 0, 10 krad, 100 krad, 500 krad, and 1 Mrad(SiO_2) under VTGL = −1.2V.

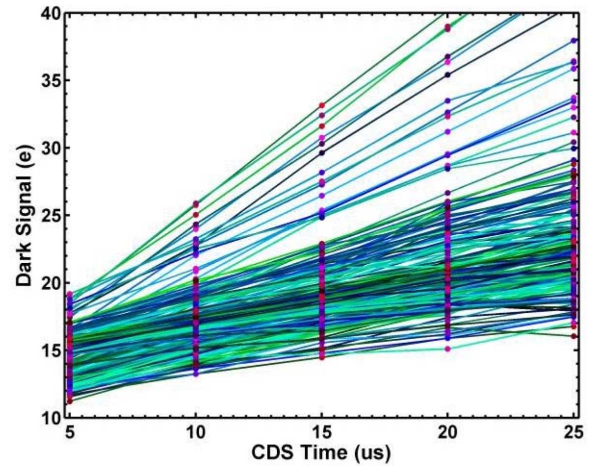

FIGURE 14. The 100-frame averaged dark signal as a function of the CDS time difference (Δt) for a set of randomly selected 200 pixels.

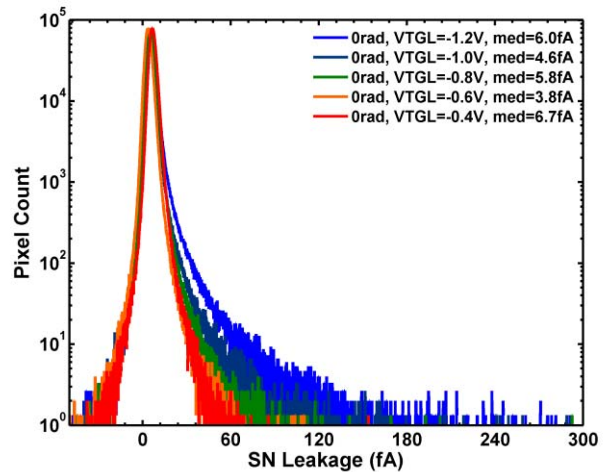

FIGURE 15. The SN leakage histograms for a chip without any X-ray irradiation under VTGL = −1.2V, −1.0V, −0.8V, −0.6V, and −0.4V.

output signal. Such an offset does not affect the DC because the DC is typically measured by subtracting one dark frame with short integration time from another dark frame with long integration time. Hence the fixed offset is cancelled.

Nevertheless, the importance of the SN leakage cannot be overlooked. To measure the SN leakage we need to look at the dark signal dependence on the CDS time difference Δt in the test mode. In addition, the TG pulses are disabled during the CDS such that no charges are transferred from PD to SN. The 100-frame averaged dark signals of 200 selected pixels as a function of Δt (from 5 to 25 μs) are plotted in Fig. 14. The SN leakage of each pixel is then calculated by a linear regression fitting of the dark signal versus Δt. A family of full array SN leakage histograms for a chip without X-ray irradiation under various VTGL is plotted in Fig. 15. Similar to the RN distributions without X-ray irradiation, for the bulk of the population the SN leakage shows very little dependence on VTGL. Only a small number of pixels on the long tails show some VTGL variation. The median SN leakage ranges from 3.8 to 6.7 fA in these measurements.

It is important to point out that the SN leakage is much higher than the DC of the photodiode. Taking the case of VTGL = −1.2 V for example, the SN leakage is about 6.0 fA, or 37,500 e/s. This value is almost 6 orders of magnitude higher than the photodiode DC at RT.

This huge disparity is due to the physical difference between the PD and the SN. Thanks to the pinned photodiode structure, where the p+ pinning layer isolates the leaky Si/SiO_2 interface from the PD junction, and to the absence of any contact region, the PD leakage is dramatically reduced. The SN leakage is much higher because the SN does not have the benefits of the pinning layer and has a leaky contact region. At RT the 6.0 fA median leakage would generate 0.94 electrons dark signal on the SN over 25 μs. But if we consider the elevated temperature and the pixels on the distribution tail, the SN leakage could be too high such that it would degrade the sensor performance. This is an area that needs improvement and the work is in progress.

The statistical distributions of the SN leakage after X-ray irradiation are plotted in Fig. 16 for VTGL = −1.2 V and in Fig. 17 for VTGL = −0.4 V, respectively. It is evident that the SN leakage increases significantly after X-ray irradiation, and the higher TID level causes higher SN leakage [43]. Similar to the RN distribution, the long tails of SN leakage can be suppressed significantly by raising VTGL from −1.2 V to −0.4 V, which is the signature of GIDL.

VI. SF-RTN AND SN GIDL-RTN WAVEFORMS

In Sections IV and V, several pieces of evidence linked the RTN generated by X-ray irradiation to the GIDL indirectly. The RN dependence on VTGL is shown in Figs. 7 and 8. The separation of the pixels dependent on VTGL from those independent of VTGL is demonstrated in Figs. 10–12.

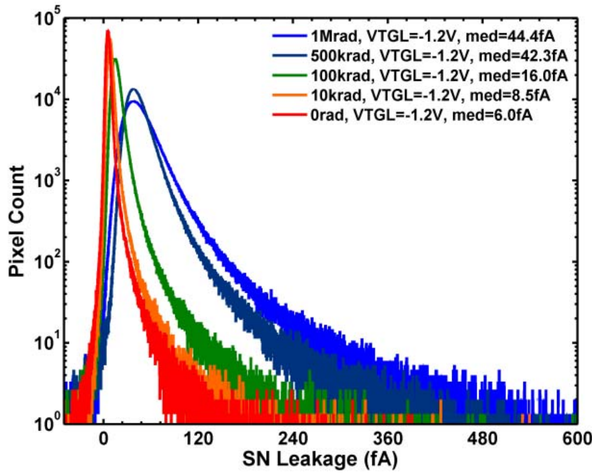

FIGURE 16. The SN leakage histograms for X-ray TID of 0, 10 krad, 100 krad, 500 krad, and 1 Mrad(SiO_2) under VTGL = −1.2V.

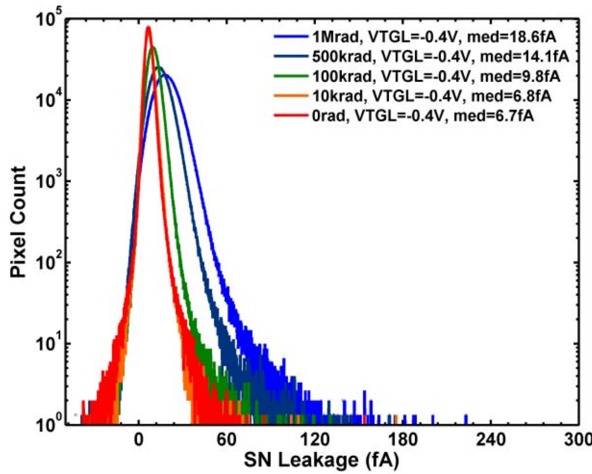

FIGURE 17. The SN leakage histograms for X-ray TID of 0, 10 krad, 100 krad, 500 krad, and 1 Mrad(SiO_2) under VTGL = −0.4V.

The SN leakage dependence on VTGL is presented in Figs. 16 and 17. The next step is to examine the direct evidence of variable GIDL-RTN by inspecting the individual pixel behavior.

The two types of RTN, the SF MC-RTN and the SN GIDL-RTN, can be distinguished based on their time domain waveforms and the dependence on CDS time Δt and VTGL. They are illustrated by the following examples.

The dark noise waveforms of three selected pixels captured with three CDS time Δt (10, 15, and 25 μs) are shown in Fig. 18. Each waveform consists of 5,000 data points sampled from consecutive frames. The waveforms of the same three pixels taken under three VTGL values (−1.2, −0.8, and −0.4 V) are shown in Fig. 19, to be side-by-side compared with Fig. 18.

The pixel in Fig. 18(a) is a typical example of the SF-RTN with a single trap. The trap may change randomly between an empty state and an occupied state with certain probabilities during the first and the second sampling.

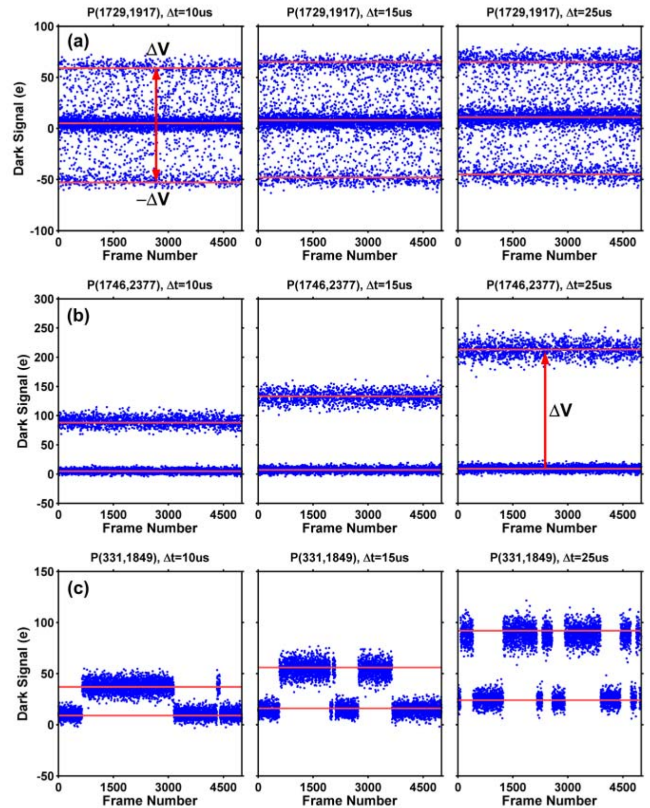

FIGURE 18. The 5,000-frame noise waveforms (captured at 1 fps) of 3 selected pixels versus CDS time difference Δt of 10, 15, and 25 μs, respectively.

The effect of the CDS subtraction results in 3 discrete signal levels. All 3 levels drift in parallel with respect to the CDS time Δt, with the upper and lower levels spaced equally apart from the center one. It means that the drift is due to a constant SN leakage and the RTN magnitude (ΔV) is independent of the CDS time Δt. The fact that the randomly distributed upper and lower levels are often observed suggests that the time constants of this type of RTN are shorter than, or comparable to, the CDS time Δt such that the trap occupancy flips frequently between the first and the second sampling.

Pixels with this type of SF-RTN are found abundant on the long RN tails of the un-irradiated samples as reported in [29]–[31]. They may account for 80-90% of the high RN pixels.

The time constant distribution of this chip reported in [29]–[31] had a median around 5 μs and ranges from 1 to 500 μs. It is noted that the time constants reported in [27] had much wider ranges than those observed in this chip. It appears that the time constants strongly depend on the technology node, device geometry, and the process details (for example, CIS or non-CIS processes).

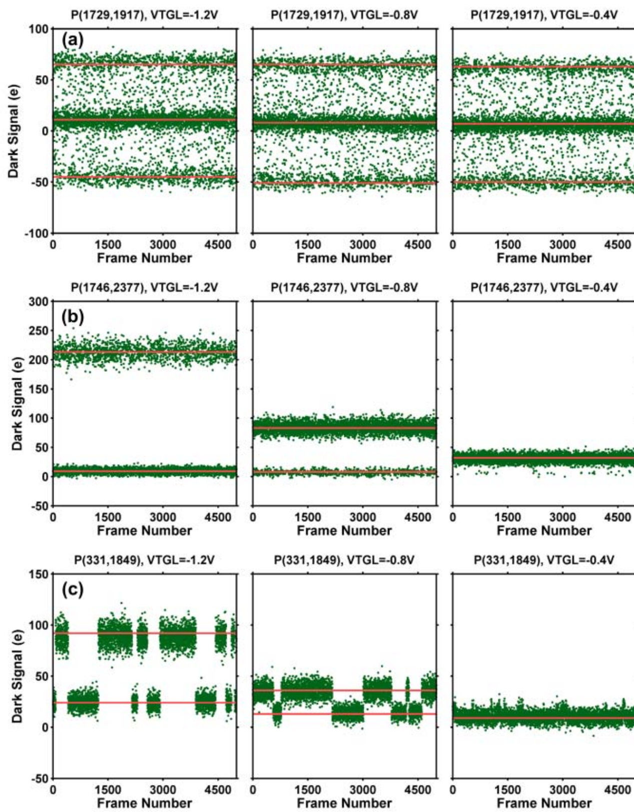

FIGURE 19. The 5,000-frame noise waveforms (captured at 1 fps) of 3 selected pixels versus VTGL of −1.2, −0.8., and −0.4 V, respectively.

The pixel in Fig. 18(b) is a representative showing a fast SN GIDL-RTS phenomenon leading to a GIDL-RTN type of noise. The 2 discrete levels drift along different slopes versus CDS time Δt, suggesting that they correspond to 2 different SN leakage currents. For this reason, the magnitude of the RTN (ΔV) is approximately proportional to Δt. The interpretation of this behavior is that the SN leakage may switch randomly between 2 different values. The time constants are likely to be longer than the CDS time such that the leakage current tends to stay at the same value during the first and the second sampling. Accordingly, only two, rather than three, discrete levels are observable. But the time constants for pixel (b) are still shorter than, or comparable to, the frame time (1 second) such that a random switching from frame to frame is obviously visible.

The pixel in Fig. 18(c) shows similar SN GIDL-RTN characteristics as the pixel (b). Yet, the time constants of pixel (c) seem to be much longer than the frame time so they could get stuck with one leakage current for many frames before switching to the other level, as it is previously reported for DC-RTS. The total capture time for 5,000 frames is about 1.4 hour at the rate of 1 frame per second. Only a few instances of switching are observed in pixel (c). On the contrary, for SF-RTN type of pixels, such long time constants are never observed in the samples tested, because such low frequency fluctuation is filtered out by the CDS.

The different RTN behavior in terms of the dependence on VTGL is further demonstrated in Fig. 19. The magnitude of the SF-RTN pixel (a) shows no dependence on VTGL. In contrast, the magnitude of the SN GIDL-RTN pixels (b) and (c) can be strongly modulated by VTGL. The physical modeling of how the electrical field between the SN and TG influences the RTN magnitude would be an interesting topic for further study.

Based on above observations, we then systematically sorted the pixels in one chip before irradiation and one chip after the 1 Mrad(SiO_2) X-ray irradiation into different RTN categories. In this report we did the sorting for the 4,000 noisiest pixels in each chip. The results are tabulated in Table 3 (before irradiation) and Table 4 (after 1 Mrad X-ray irradiation).

TABLE 3. Chip before irradiation.

Random Noise Histogram Types	ALL pixels		SN GIDL pixels	
	Number	Percent	Number	Percent
1 peak (non RTN)	562	14.1%	0	0.0%
2 peaks (RTN)	89	2.2%	8	0.2%
3 peaks (RTN)	3349	83.7%	0	0.0%
Total	4000	100%	8	0.2%

TABLE 4. Chip after 1 Mrad(SiO_2) X-ray irradiation.

Random Noise Histogram Types	ALL pixels		SN GIDL pixels	
	Number	Percent	Number	Percent
1 peak (non RTN)	139	3.5%	74	1.9%
2 peaks (RTN)	3338	83.5%	3338	83.5%
3 peaks (RTN)	523	13.1%	66	1.7%
Total	4000	100%	3478	87.0%

We first identified the number of peaks in the signal histograms, and labeled the GIDL-RTN pixels by 2 criteria: (1) whether the RTN amplitude is proportional to the CDS time Δt; (2) whether the RTN amplitude can be suppressed by changing VTGL from −1.2 V to −0.4 V.

The most interesting finding by comparing Tables 3 and 4 is that the SN GIDL-RTN pixels are very rare in the sample without irradiation. But they become abundant and dominant in the sample irradiated X-ray at 1 Mrad(SiO_2) level.

For the chip without irradiation, the dominant RTN type among the noisiest 4,000 pixels is the SF-RTN (83.7%) and almost no SN GIDL-RTN pixels. The striking difference in the irradiated chip is that the dominant RTN type becomes the SN GIDL-RTN (83.5%) and the percentage of SF-RTN pixels is relatively lower (13.1%).

VII. CONCLUSION

In our previous study of the same 8.3 MP, 1.1 um pixel CIS [29]–[31] without any intentional radiation exposure, the long tail of the RN distribution was dominated by pixels with single-trap SF-RTN showing 3 distinct and symmetrically

spaced discrete levels. In this X-ray irradiation experiment, we found that the pixels with highest noises are dominated by the SN GIDL-RTN.

These two types of RTN behaviors are quite distinguishable. The magnitude of the SN GIDL-RTN is linearly proportional to the CDS time Δt, while the SF-RTN is relatively independent of Δt, as long as the CDS time is longer than the circuit settling time and the SF-RTN time constants [29]–[31]. The magnitude of the variable GIDL-RTN can be suppressed by reducing the electric field between the SN and the TG, but the SF-RTN is not affected by the VTGL. It is evident that the number of pixels with variable GIDL-RTN increases as the X-ray TID increases.

It seems the time constants of the variable GIDL-RTN have very wide ranges. Some are so long that only a few switching is observed during 1.4 hours. It implies that a much longer observing time is needed for accurate time constant extraction based on the switching statistics. Some GIDL-RTN time constants are shorter than the 1 second frame time but longer than the 25 μs CDS time such that a frequent random switching between 2 discrete levels is observed in the waveforms. The systematic extraction of the GIDL-RTN time constants would be a potential topic for future work.

In summary, we reported for the first time a systematic study on the RTN caused by variable TG-induced SN leakage, as well as the measurement results of the statistical distributions of the RN, the DC, and the SN leakage before and after X-ray irradiation and their dependence on CDS time and VTGL. We presented several methods to differentiate the SN GIDL-RTN pixels from the SF MC-RTN pixels using scatter plots, 2D histograms, and the time-domain waveforms.

The RTN remains to be a fascinating and fruitful subject to study in device engineering. For CIS manufacturing, it is a continuing objective to identify and to eliminate the sources of RTN due to any process induced damage.

REFERENCES

[1] S. Takahashi *et al.*, "A 45 nm stacked CMOS image sensor process technology for submicron pixel," *Sensors*, vol. 17, no. 12, 2017, Art. no. 2816.

[2] S. Takahashi *et al.*, "Low dark current and low noise 0.9 μm pixel in a 45 nm stacked CMOS image sensor process technology," in *Proc. Int. Image Sensor Workshop (IISW)*, Hiroshima, Japan, May 2017, pp. 16–19.

[3] Y. Kim *et al.*, "A 1/2.8-inch 24Mpixel CMOS image sensor with 0.9μm unit pixels separated by full-depth deep-trench isolation," in *Proc. IEEE Int. Solid-State Circuit Conf. (ISSCC)*, San Francisco, CA, USA, Feb. 2018, pp. 84–85.

[4] V. C. Venezia *et al.*, "Second generation small pixel technology using hybrid bond stacking," *Sensors*, vol. 18, no. 2, 2018, Art. no. 667.

[5] Sony News Releases. (Jul. 28, 2018). *Sony Releases Stacked CMOS Image Sensor for Smartphones With Industry's Highest 48 Effective Megapixels, Featuring World First Ultra-Compact Pixel Size of 0.8 μm*. [Online]. Available: https://www.sony.net/SonyInfo/News/Press/201807/18-060E/index.html

[6] E. Simoen and C. Claeys, *Random Telegraph Signals in Semiconductor Devices*. Bristol, U.K.: IOP Publ. Ltd., 2016.

[7] N. Teranishi, A. Kohono, Y. Ishihara, E. Oda, and K. Arai, "No image lag photodiode structure in the interline CCD image sensor," in *Proc. IEEE Int. Electron Devices Meeting (IEDM)*, San Francisco, CA, USA, Dec. 1982, pp. 324–327.

[8] E. R. Fossum and D. B. Hondongwa, "A review of pinned photodiode for CCD and CMOS image sensors," *IEEE J. Electron Devices Soc.*, vol. 2, no. 3, pp. 33–43, May 2014.

[9] N. Teranishi, "Effect and limitation of pinned photodiode," *IEEE Trans. Electron Devices*, vol. 63, no. 1, pp. 10–15, Jan. 2016.

[10] Y. Mori, K. Ohyu, K. Okonogi, and R. Yamada, "The origin of variable retention time in DRAM," in *Proc. IEEE Int. Electron Devices Meeting (IEDM)*, Baltimore, MD, USA, Dec. 2005, pp. 1–4.

[11] K. Ohyu *et al.*, "Quantitative identification for the physical origin of variable retention time: A vacancy-oxygen complex defect model," in *Proc. IEEE Int. Electron Devices Meeting (IEDM)*, San Francisco, CA, USA, Dec. 2006, pp. 1–4.

[12] H. Silva and S. Tiwari, "Random telegraph signals in nanoscale back-side charge trapping memories," *Appl. Phys. Lett.*, vol. 88, no. 10, pp. 1–3, Mar. 2006.

[13] H. Kim *et al.*, "RTS-like fluctuation in gate induced drain leakage current of Saddle-Fin type DRAM cell transistor," in *Proc. IEEE Int. Electron Devices Meeting (IEDM)*, Baltimore, MD, USA, Dec. 2009, pp. 1–4.

[14] J.-W. Lee, B. H. Lee, H. Shin, and J.-H. Lee, "Investigation of random telegraph noise in gate-induced drain leakage and gate edge direct tunneling currents of high-k MOSFETs," *IEEE Trans. Electron Devices*, vol. 57, no. 4, pp. 913–918, Apr. 2010.

[15] J.-W. Lee, H. Shin, and J.-H. Lee, "Characterization of random telegraph noise in gate induced drain leakage current of *n*- and *p*-type metal–oxide–semiconductor field–effect transistors," *Appl. Phys. Lett.*, vol. 96, pp. 1–3, Jan. 2010.

[16] Y. Mori, K. Takeda, and R.-I. Yamada, "Random telegraph noise of junction leakage current in submicron devices," *J. Appl. Phys.*, vol. 107, pp. 1–10, Jan. 2010.

[17] B. Oh *et al.*, "Characterization of an oxide trap leading to random telegraph noise in gate-induced drain leakage current of DRAM cell transistors," *IEEE Trans. Electron Devices*, vol. 58, no. 6, pp. 1741–1747, Jun. 2011.

[18] S. Shimizu *et al.*, "Comprehensive study of systematic and random variation in gate-induced drain leakage for LSTP applications," in *Proc. IEEE Symp. VLSI Technol. (VLSI-T)*, Kyoto, Japan, Jun. 2011, pp. 196–197.

[19] Y. Mori, H. Yoshimoto, K. Takeda, and R. Yamada, "Mechanism of random telegraph noise in junction leakage current of metal–oxide–semiconductor field–effect transistor," *J. Appl. Phys.*, vol. 111, no. 10, pp. 1–9, May 2012.

[20] S.-W. Yoo, Y. Son, and H. Shin, "Capture cross section of traps causing random telegraph noise in gate-induced drain leakage current," *IEEE Trans. Electron Devices*, vol. 60, no. 3, pp. 1268–1271, Mar. 2013.

[21] X. Wang, P. R. Rao, A. Mierop, and A. J. P. Theuwissen, "Random telegraph signal in CIS pixels," in *Proc. IEEE Int. Electron Devices Meeting (IEDM)*, San Francisco, CA, USA, Dec. 2006, pp. 115–118.

[22] X. Wang, M. F. Snoeij, P. R. Rao, A. Mierop, and A. J. P. Theuwissen, "A CMOS image sensor with a buried-channel source follower," in *Proc. IEEE Int. Solid-State Circuits Conf. (ISSCC)*, San Francisco, CA, USA, Feb. 2008, pp. 62–63.

[23] Y. Chen, X. Wang, A. J. Mierop, and A. J. P. Theuwissen, "A CMOS image sensor with in-pixel buried-channel source follower and optimized row selector," *IEEE Trans. Electron Devices*, vol. 56, no. 11, pp. 2390–2397, Nov. 2009.

[24] P. Martin-Gonthier, V. Goiffon, and P. Magnan, "In-pixel source follower transistor RTS noise behavior under ionizing radiation in CMOS image sensors," *IEEE Trans. Electron Devices*, vol. 59, no. 6, pp. 1686–1692, Jun. 2012.

[25] K. Abe *et al.*, "Analysis of source follower random telegraph signal using nMOS and pMOS array TEG," in *Proc. Int. Image Sensor Workshop (IISW)*, Ogunquit, ME, USA, Jun. 2007, pp. 62–65.

[26] R. Kuroda *et al.*, "A statistical evaluation of random telegraph noise of in-pixel source follower equivalent surface and buried channel transistors," *IEEE Trans. Electron Devices*, vol. 60, no. 10, pp. 3555–3561, Oct. 2013.

[27] T. Obara *et al.*, "Extraction of time constants ratio over nine orders of magnitude for understanding random telegraph noise in MOSFETs," *Jpn. J. Appl. Phys.*, vol. 53, no. 4, pp. 1–7, Mar. 2014.

[28] R. Kuroda, A. Teramoto, and S. Sugawa, "Random telegraph noise measurement and analysis based on arrayed test circuit toward high S/N CMOS image sensors," in *Proc. Int. Conf. Microelectron. Test Struct. (ICMTS)*, Yokohama, Japan, Mar. 2016, pp. 46–51.

[29] C. Y.-P. Chao *et al.*, "CMOS image sensor random telegraph noise time constant extraction from correlated to uncorrelated double sampling," *IEEE J. Electron Devices Soc.*, vol. 5, no. 1, pp. 79–89, Jan. 2017.

[30] C. Y.-P. Chao *et al.*, "Random telegraph noise pixel classification and time constant extraction for a 1.1 μm pitch 8.3 MP CMOS image sensor," in *Proc. IEEE Int. Image Sensor Workshop (IISW)*, Hiroshima, Japan, May 2017, pp. 35–38.

[31] C. Y.-P. Chao *et al.*, "Statistical analysis of the random telegraph noise in a 1.1 μm pixel, 8.3 MP CMOS image sensor using on-chip time constant extraction method," *Sensors*, vol. 17, no. 2, 2017, Art. no. 2704.

[32] I. H. Hopkins and G. R. Hopkinson, "Random telegraph signals from proton-irradiated CCDs," *IEEE Trans. Nucl. Sci.*, vol. 40, no. 6, pp. 1567–1574, Dec. 1993.

[33] V. Goiffon *et al.*, "Multilevel RTS in proton irradiated CMOS image sensors manufactured in a deep submicron technology," *IEEE Trans. Nucl. Sci.*, vol. 56, no. 4, pp. 2132–2141, Aug. 2009.

[34] V. Goiffon, P. Magnan, P. Martin-Gonthier, C. Virmontois, and M. Gaillardin, "Evidence of a novel source of random telegraph signal in CMOS image sensors," *IEEE Electron Devices Lett.*, vol. 32, no. 6, pp. 773–775, Jun. 2011.

[35] V. Goiffon, C. Virmontois, and P. Magnan, "Investigation of dark current random telegraph signal in pinned photodiode CMOS image sensors," in *Proc. IEEE Int. Electron Devices Meeting (IEDM)*, Washington, DC, USA, Dec. 2011, pp. 1–4.

[36] C. Virmontois *et al.*, "Total ionizing dose versus displacement damage dose induced dark current random telegraph signals in CMOS image sensors," *IEEE Trans. Nucl. Sci.*, vol. 58, no. 6, pp. 3085–3094, Dec. 2011.

[37] V. Goiffon, P. Magnan, P. Martin-Gonthier, C. Virmontois, and M. Gaillardin, "New source of random telegraph signal in CMOS image sensors," in *Proc. IEEE Int. Image Sensor Workshop (IISW)*, Hokkaido, Japan, Jun. 2011, pp. 212–215.

[38] E. Martin, T. Nuns, C. Virmontois, J.-P. David, and O. Gilard, "Proton and γ-rays irradiation-induced dark current random telegraph signal in a 0.18μm CMOS image sensor," *IEEE Trans. Nucl. Sci.*, vol. 60, no. 4, pp. 2503–2510, Aug. 2013.

[39] C. Virmontois *et al.*, "Dark current random telegraph signals in solid-state image sensors," *IEEE Trans. Nucl. Sci.*, vol. 60, no. 6, pp. 4323–4331, Dec. 2013.

[40] C. Durnez *et al.*, "In-depth analysis on radiation induced multi-level dark current random telegraph signal in silicon solid state image sensors," *IEEE Trans. Nucl. Sci.*, vol. 64, no. 1, pp. 19–26, Jan. 2017.

[41] C. Durnez *et al.*, "Localization of dark current random telegraph signal sources in pinned photodiode CMOS image sensors," in *Proc. Int. Conf. Noise Fluctuations (ICNF)*, Vilnius, Lithuania, Jun. 2017, pp. 131–134.

[42] C. Durnez *et al.*, "Total ionizing dose radiation-induced dark current random telegraph signal in pinned photodiode CMOS image sensors," *IEEE Trans. Nucl. Sci.*, vol. 65, no. 1, pp. 92–100, Jan. 2018.

[43] A. Le Roch *et al.*, "Radiation induced leakage current and electric field enhancement in CMOS image sensor floating diffusions," *IEEE Trans. Nucl. Sci.*, to be published, doi: 10.1109/TNS.2019.2892645.

[44] T.-H. Tsai, D. Marchesan, N. Faramarzpour, M. Sonder, and E. Fox, "Twinkling behavior in ultra-high-resolution CMOS global shutter pixels," in *Proc. IEEE Int. Image Sensor Workshop (IISW)*, Vaals, The Netherlands, Aug. 2015, pp. 98–101.

[45] B. Pain, T. Cunningham, B. Hancock, C. Wrigley, and C. Sun, "Excess noise and dark current mechanisms in CMOS imagers," in *Proc. IEEE Workshop CCD Adv. Image Sensor*, Nagano, Japan, Jun. 2005, pp. 153–156.

[46] B. Pain, B. Hancock, C. Sun, and C. Wrigley, "Twinkling pixels: Random telegraph signals at reset gate edge," in *Proc. IEEE Int. Image Sensor Workshop (IISW)*, Ogunquit, ME, USA, Jun. 2007, pp. 234–237.

[47] A. Theuwissen, J. Bosiers, and E. Roks, "The hole role," in *Proc. IEEE Int. Electron Devices Meeting (IEDM)*, Washington, DC, USA, Dec. 2005, pp. 817–820.

[48] A. J. Theuwissen, "The hole role in solid-state imagers," *IEEE Trans. Electron Devices*, vol. 53, no. 12, pp. 2972–2980, Dec. 2006.

[49] H. Han *et al.*, "Evaluation of a small negative transfer gate bias on the performance of 4T CMOS image sensor pixels," in *Proc. IEEE Int. Image Sensor Workshop (IISW)*, Ogunquit, ME, USA, Jun. 2007, pp. 238–240.

[50] B. Mheen, Y.-J. Song, and A. J. P. Theuwissen, "Negative offset operation of four-transistor CMOS image pixels for increased well capacity and suppressed dark current," *IEEE Electron Devices Lett.*, vol. 29, no. 4, pp. 347–349, Apr. 2008.

[51] H. Yamashita, M. Maeda, S. Furuya, and T. Yagami, "Analysis of dark current in 4-transistor CMOS imager pixel with negative transfer-gate bias operation," in *Proc. IEEE Int. Image Sensor Workshop (IISW)*, Bergen, Norway, Jun. 2009, pp. 24–27.

[52] T. Watanabe, J.-H. Park, S. Aoyama, K. Isobe, and S. Kawahito, "Effects of negative-bias operation and optical stress on dark current in CMOS image sensors," *IEEE Trans. Electron Devices*, vol. 57, no. 7, pp. 1512–1518, Jul. 2010.

[53] H. Yamashita, M. Maeda, S. Furuya, and T. Yagami, "Dark noise in a CMOS imager pixel with negative bias on transfer gate," in *Proc. SPIE*, vol. 7875, Feb. 2011, Art. no. 78750J. [Online]. Available: http://spie.org/Publications/Proceedings/Paper/10.1117/12.876368, doi: 10.1117/12.876368.

[54] C. Y.-P. Chao *et al.*, "Extraction and estimation of pinned photodiode capacitance in CMOS image sensors," *IEEE J. Electron Devices Soc.*, vol. 2, no. 4, pp. 59–64, Jul. 2014.

CALVIN YI-PING CHAO received the M.S. and Ph.D. degrees in electrical and computer engineering from the University of Illinois at Urbana–Champaign, IL, USA, in 1987 and 1992, respectively. He was with MicroMedia, Inc., e-Phocus, Inc., Burr-Brown Corporation, and IBM Microelectronics, on diverse projects, including CIS design, image processing, analog and mixed-signal IC design, device modeling, characterization, reliability physics, and process development. He is currently a Deputy Director of the Mixed Signal and RF Solution Division, Research and Development, TSMC. He has authored 33 U.S. patents and 31 papers.

THOMAS M.-H. WU received the B.S. and M.S. degrees in engineering science from National Cheng Kung University, Tainan, Taiwan, in 2000 and 2003, respectively. From 2004 to 2008, he was an Assistant Researcher with the Instrument Technology Research Center, National Applied Research Laboratories, Hsinchu, Taiwan. In 2014, he joined TSMC. His research interest includes CMOS image sensor characterization, applications, and systems.

SHANG-FU YEH received the B.S. and M.S. degrees in electrical engineering from National Central University, Zhongli, Taiwan, in 2001 and 2003, respectively, and the Ph.D. degree in electrical engineering from National Tsing Hua University, Hsinchu, Taiwan, in 2014. From 2003 to 2008, he designed IO, low dropout regulators, and high speed interface circuits with EE-Solutions, Inc., Hsinchu. In 2012, he joined TSMC, where he is currently a Mixed-Signal Circuit Designer. His research interests include low noise and high speed CMOS image sensors design.

KUO-YU CHOU received the B.S. and M.S. degrees in communication engineering from National Chiao Tung University, Hsinchu, Taiwan, in 1996 and 1998, respectively. He is specialized in high speed ADC, low noise circuit, and CMOS image sensor designs. He is currently a Design Manager of the CIS Design Program in TSMC.

HONYIH TU received the B.S. degree in electrical engineering from National Central University, Zhongli, Taiwan, in 1993. From 1995 to 2005, he was a Designer, a Project Leader, and a Product Manager for digital still cameras. From 2006 to 2009, he engaged in CIS ISP development, turnkey solutions, and customer support. He joined TSMC in 2010, where he is responsible for system software and hardware integration for CIS characterization. His interests include image sensor applications, imaging systems, and ISP algorithm development.

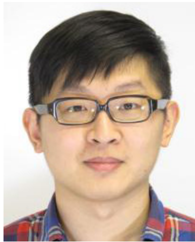

CHIH-LIN LEE received the B.S. degree in electronics engineering from Chung Yuan Christian University, Zhongli, Taiwan, in 2008 and the M.S. and Ph.D. degrees in electrical engineering from National Tsing Hua University, Hsinchu, Taiwan, in 2010 and 2014, respectively. He joined TSMC in 2015, where he is responsible for CIS, analog and mixed-signal IC design. His research interests include low noise CMOS image sensors design and high speed CMOS image sensors design.

CHIN YIN received the B.S., M.S., and Ph.D. degrees from National Tsing Hua University, Hsinchu, Taiwan, in 2009, 2010, and 2017, respectively. He joined TSMC in 2017, where he is currently a Mixed-Signal Circuit Designer. His research interests include low noise CMOS image sensors and SPAD ToF sensors design.

PHILIPPE PAILLET (M’97–SM’04–F’18) received the master’s degree in electrical engineering from the Universiteé Aix-Marseille I, France, in 1989 and the Ph.D. degree in electrical engineering from the Université Montpellier II, France, in 1995. He joined the Commissariat à l’Energie Atomique, Arpajon, France, in 1995, where he is a Senior Member of the Technical Staff and a Project Manager. He has been involved in numerous programs developing radiation-hardened electronic and optoelectronic technologies, characterizing the physical mechanisms responsible for radiation response of components and ICs, modeling the effects of radiation in MOS technologies and the creation of radiation-induced defects, and developing hardness assurance approaches. He has authored or co-authored over 200 publications, articles, short courses, and book chapters. He was a recipient of two Best Papers at RADECS, two Meritorious Paper Awards at NSREC, one Best Paper Award at HEART, and five Outstanding Paper Awards at NSREC for his authored or co-authored papers. He is currently serving as the Vice-President of the RADECS Association (the Steering Group of RADECS Conferences) and RADECS Liaison to the IEEE Radiation Effects Steering Group.

VINCENT GOIFFON (S’08–M’09) received the M.S. degree in aerospace engineering and the Ph.D. degree in electrical engineering from ISAE-SUPAERO, University of Toulouse, Toulouse, France, in 2005 and 2008, respectively, where he has been with the Image Sensor Research Group and is currently a Full Professor. His research interests include solid state image sensors, CMOS integrated circuit design, pixel modeling/simulation/characterization, leakage/dark current, random telegraph signals, radiation effects, and hardening-by-design techniques. He is regularly involved in scientific image sensor research and development projects, especially for space and nuclear applications. He has authored or co-authored one book chapter and over 60 journal papers. He was a recipient of one NSREC Outstanding Conference Paper Award and four Outstanding Student Paper Awards (at IEEE NSREC and RADECS conferences) for his authored or co-authored papers.